(Supporting Information)

Band-Tail Transport of CuSCN: Origin of Hole Extraction Enhancement in Organic Photovoltaics

Minju Kim,[†] Soohyung Park,[†] Junkyeong Jeong,[†] Dongguen Shin,[†] Jimin Kim,[‡,||] Sae Hee Ryu,[‡,||] Keun Su Kim,[‡,||] Hyunbok Lee,[,§] and Yeonjin Yi[*,†]*

[†]Institute of Physics and Applied Physics, Yonsei University, 50 Yonsei-ro, Seodaemun-gu, Seoul 03722, Korea

[‡]Department of Physics, Pohang University of Science and Technology, Pohang 37673, Korea

[§]Department of Physics, Kangwon National University, 1 Gangwondaehak-gil, Chuncheon-si, Gangwon-do 24341, Korea

[||]Center for Artificial Low Dimensional Electronic Systems, Institute for Basic Science, Pohang 37673, Korea

Corresponding Authors:

[*]E-mail: hyunbok@kangwon.ac.kr (H. L.)

[*]E-mail: yeonjin@yonsei.ac.kr (Y.Y.)

1. Morphology and cross-sectional image of the spin-coated CuSCN films

Figure S1 shows AFM images of bare ITO and spin-coated CuSCN films on ITO with various solution concentrations. Generally, the CuSCN films show the island-like growth and the CuSCN film formed with a 20 mg ml^{-1} concentration shows good quality. This is similar to the nanocrystalline film reported.[1,2] The thickness of a 20 mg ml^{-1} film was measured to be 100 nm by a cross-sectional SEM (JEOL Ltd, JEOL-7001F, Figure S2) and a surface profiler (KLA Tencor, Alpha-step 500). This film was used for the electronic structure measurements.

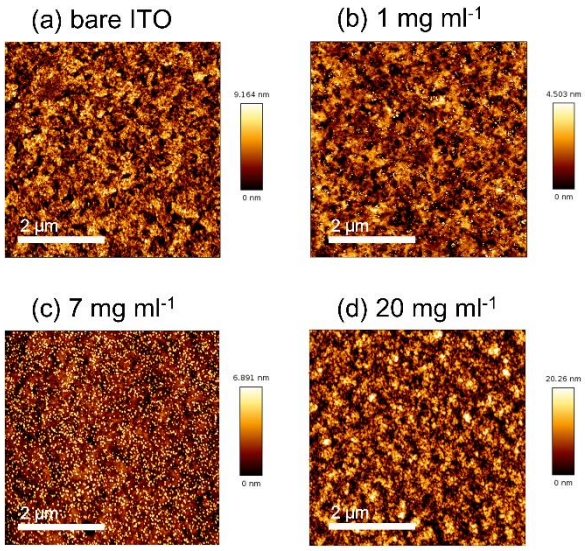

Figure S1. AFM images of (a) the bare ITO substrate and CuSCN films on ITO formed with various solution concentrations of (b) 1 mg ml^{-1}, (c) 7 mg ml^{-1} and (d) 20 mg ml^{-1}.

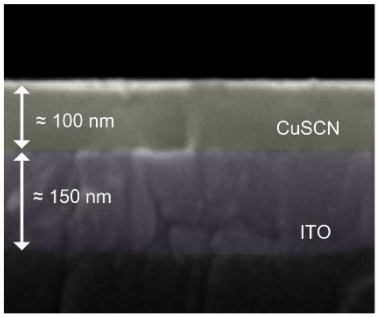

Figure S2. Cross-sectional SEM image of the spin-coated CuSCN film formed with a 20 mg ml^{-1} solution on the ITO substrate.

2. UPS spectra of the spin-coated CuSCN films

Figure S3 shows the measured UPS spectra of bare ITO and spin-coated CuSCN films on ITO from various solution concentrations (1, 7, 20 mg ml^{-1}). This makes it possible to observe the thickness-dependent energy level changes. It shows an abrupt change in a secondary electron cutoff (SEC) with varying the CuSCN thickness (controlled by its concentration), meaning the formation of an interface dipole (eD). On the other hand, the valence band maximum (VBM) hardly changes with increasing the CuSCN thickness, which means a negligible space charge layer in CuSCN. Collectively inferring, the E_F equilibrium could be fully established with the eD (E_F pinning) through enough density of states (DOS) of tail states.

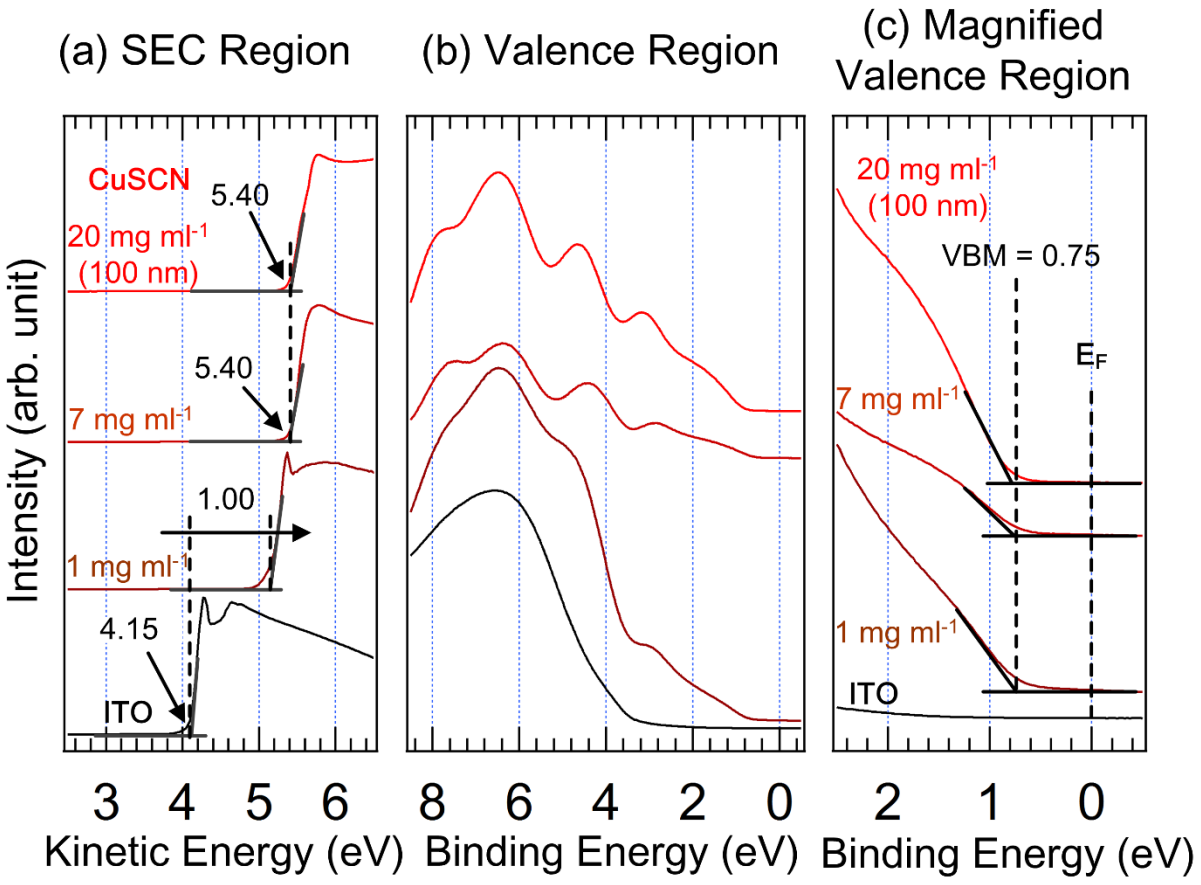

Figure S3. UPS spectra of the bare ITO substrate and the spin-coated CuSCN films on the ITO substrate with various solution concentrations (1, 7, 20 mg ml^{-1}). Each panel shows (a) the normalized SEC region, (b) the background and He I_β satellite-removed valence region and (c) the magnified valence region.

3. Determination on the valence band maximum of CuSCN

We performed density functional theory (DFT) calculations with Vienna Ab initio Simulation Package (VASP) 5.2 to determine the valence band edge reasonably. We represented the wave function in a projector-augmented wave basis with an energy cutoff of 500 eV. The generalized gradient approximation (GGA) density functional of Perdew-Burke-Ernzerhof (PBE) was used. The electronic iteration convergence condition was 1.0×10^{-6} eV and a 9×9×3 *k*-space grid was employed. Geometry optimization for the β-phase CuSCN unit cell was carried out until the change of forces becomes less than 0.01 eV $Å^{-1}$. Since it is reported that β-CuSCN is more stable and is obseved at the films, we considered only β-CuSCN here.[3–5]

Figure S4 below shows (a) the calculated band structure of β-CuSCN, (b) the calculated DOS of β-CuSCN and (c) comparison between the calculated DOS of β-CuSCN with the E_F correction (violet line) and the measured CuSCN UPS spectrum (black line). As shown in Figures S4a and S4b, the VBM is located at the Γ point, which is at 0.10 eV below the calculated E_F. The calculated E_F was determined from the chemical potential of our model. To match the calculated E_F with the measured E_F, the energetic shift of 0.70 eV was applied, which was determined from the energetic difference between the characteristic features of the calculated DOS and measured UPS spectrum (marked as A and B in Figure S4c). This originates from the E_F difference between DFT calculations and UPS measurements. As a result, the calculated DOS with the E_F correction and the meausred UPS spectrum are in excellent agreement for all valence region as shown in Figure S4c, although we did not apply any stretch or compression for energy levels. Therefore, we determined the refined theoretical VBM (0.80 eV) with the E_F correction (0.70 eV) into the calculated pristine VBM (0.10 eV) which matches well with the measured VBM (0.75 eV) within the experimental error.

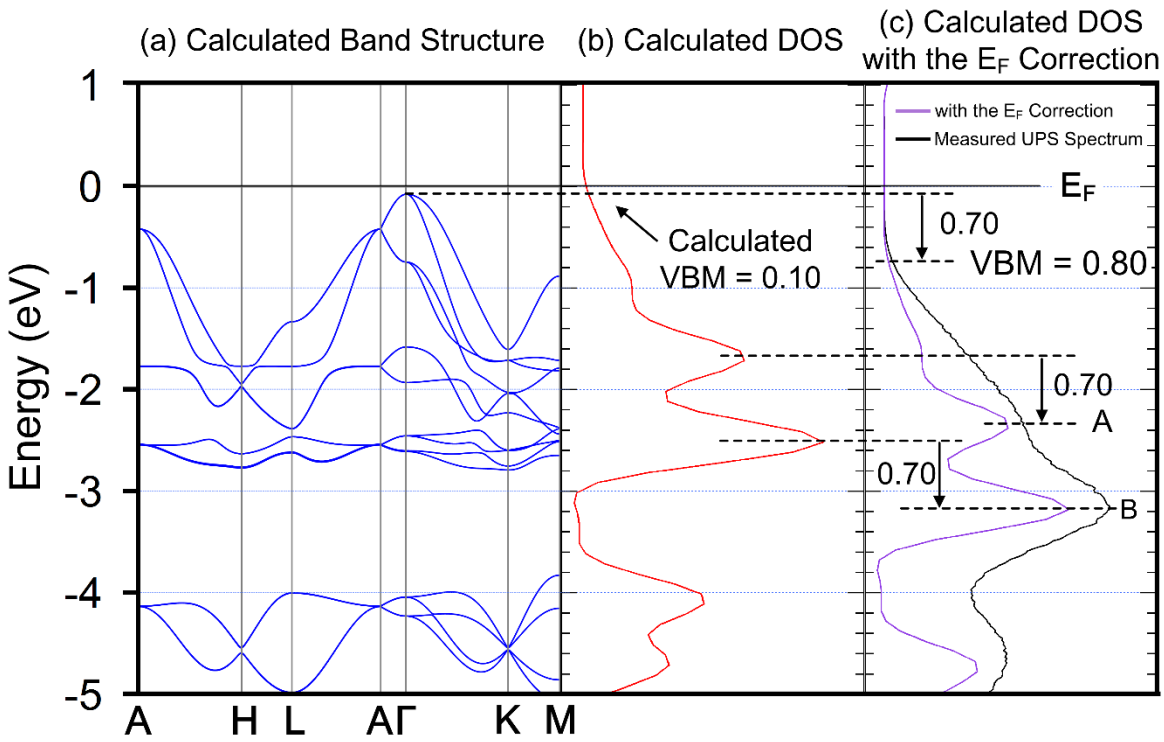

Figure S4. (a) The calculated band structure of β-CuSCN, (b) the calculated density of states (DOS) of β-CuSCN and (c) comparison between the calculated DOS of β-CuSCN with the E_F correction (violet line) and the measured CuSCN UPS spectrum (black line).

4. Calculation of the film thickness

We calculated the thicknesses of VESD-deposited P3HT films using the electron effective attenuation length (EAL) of N 1s and In $3d_{5/2}$ XPS spectra.

$$\frac{I}{I_0} = e^{\frac{-d}{\lambda}}$$

$$(I: photoelectron\ intensity\ of\ film,\ I_0: photoelectron\ intensity\ of\ substrate,$$
$$d: film\ thickness, \lambda: effective\ attenuation\ length\ )$$

.

EALs were calculated using the NIST Electron Effective-Attenuation-Length Database with our experimental parameters such as photoelectron kinetic energy (1088 eV for N 1s and 1043 eV for In 3d), incident angle (70°), emission angle (20°) and inelastic mean free path of P3HT. ($IMFP_{P3HT}$, N 1s = 29.9 Å, $IMFP_{P3HT}$, In 3d = 28.9 Å)[6]

Figure S5 shows the measured XPS spectra of N 1s during the interface formation of P3HT/CuSCN. I_0 is the N 1s intensity of CuSCN and I is its attenuated intensity during the P3HT deposition. Table S1 shows the calculated thicknesses of P3HT. Figure S6 shows the measured XPS spectra of In $3d_{5/2}$ during the interface formation of P3HT/ITO. In this case, I_0 is the In $3d_{5/2}$ intensity of ITO and I is its attenuated intensity during the P3HT deposition. Table S2 shows the calculated thicknesses of P3HT.

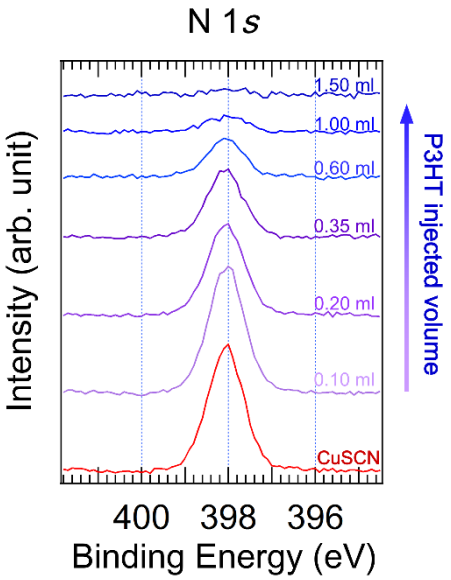

Figure S5. XPS spectra of N 1s during the interface formation of P3HT/CuSCN.

Table S1. The calculated P3HT film thicknesses from photoelectron intensities of the XPS N 1s spectrum and the injected volumes of a P3HT solution.

P3HT/CuSCN/ITO (N 1s peak)		
injected volume (ml)	N 1s intensity (arb. unit)	calculated thickness (nm)
0.00	1617	0
0.10	1550	0.1
0.20	1134	1.0
0.35	870	1.7
0.60	467	3.5
1.00	234	5.5
1.50	78	8.6

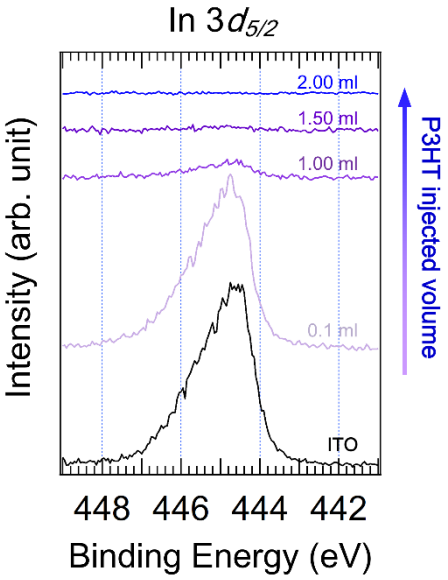

Figure S6. XPS spectra of In $3d_{5/2}$ during the interface formation of P3HT/ITO.

Table S2. The calculated P3HT film thicknesses from photoelectron intensities of the XPS In $3d_{5/2}$ spectrum and the injected volumes of a P3HT solution.

P3HT/ITO [In $3d_{5/2}$ peak]		
injected volume (ml)	In $3d_{5/2}$ intensity (arb. unit)	calculated thickness (nm)
0.00	1482	0
0.10	1417	0.1
1.00	206	5.4
1.50	104	7.3
2.00	20	11.7

5. XPS S 2p spectra at the interface of P3HT/CuSCN

Figure S7 shows the measured XPS spectra of S 2p core level during the formation of a P3HT/CuSCN interface. We fitted the S 2p spectra with two components of the pristine (bulk) CuSCN (red line) and P3HT (blue line) after background removal. Although we could not see the subtle shape change from these fittings, the rigid energy level shift in the P3HT overlayer was observed. This indicates that there is definite charge transfer from P3HT to CuSCN, which accords well with the energy level shift in the UPS spectra.

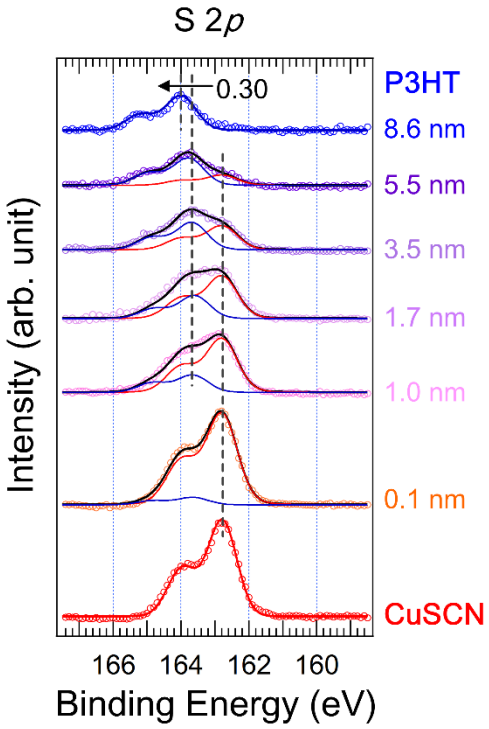

Figure S7. (a) XPS spectra of S 2p levels of the P3HT (1.0, 1.7, 3.5, 5.5, 8.6 nm) deposited on the CuSCN film. The circles and the lines indicate the measured and fitted spectra, respectively. The S 2p spectra were deconvoluted with the bulk spectra of P3HT (blue line) and CuSCN (red line).

6. Investigation on the interfacial electronic structure of P3HT/ITO

Figure S8 shows the measured UPS spectra of the (a) SEC region, (b) valence region and (c) HOMO region of P3HT (0.1, 5.4, 7.3, 11.7 nm) deposited on the ITO substrate. The work function (Ψ) of the pristine ITO was measured to be 4.00 eV as shown in Figure S8a. While the thickness of the P3HT layer increased, the SEC shifted toward lower kinetic energies by 0.60 eV. The Ψ of the 11.7 nm-P3HT layer was 3.40 eV. In Figure S8c, The HOMO onset of the 5.4 nm-P3HT layer was observed at 0.55 eV. The HOMO onset of P3HT moved gradually to higher binding energies by 0.35 eV as the P3HT layer thickened. This indicates that the band bending (V_b) of 0.35 eV occurred in the P3HT side and the eD was evaluated to be 0.25 eV.

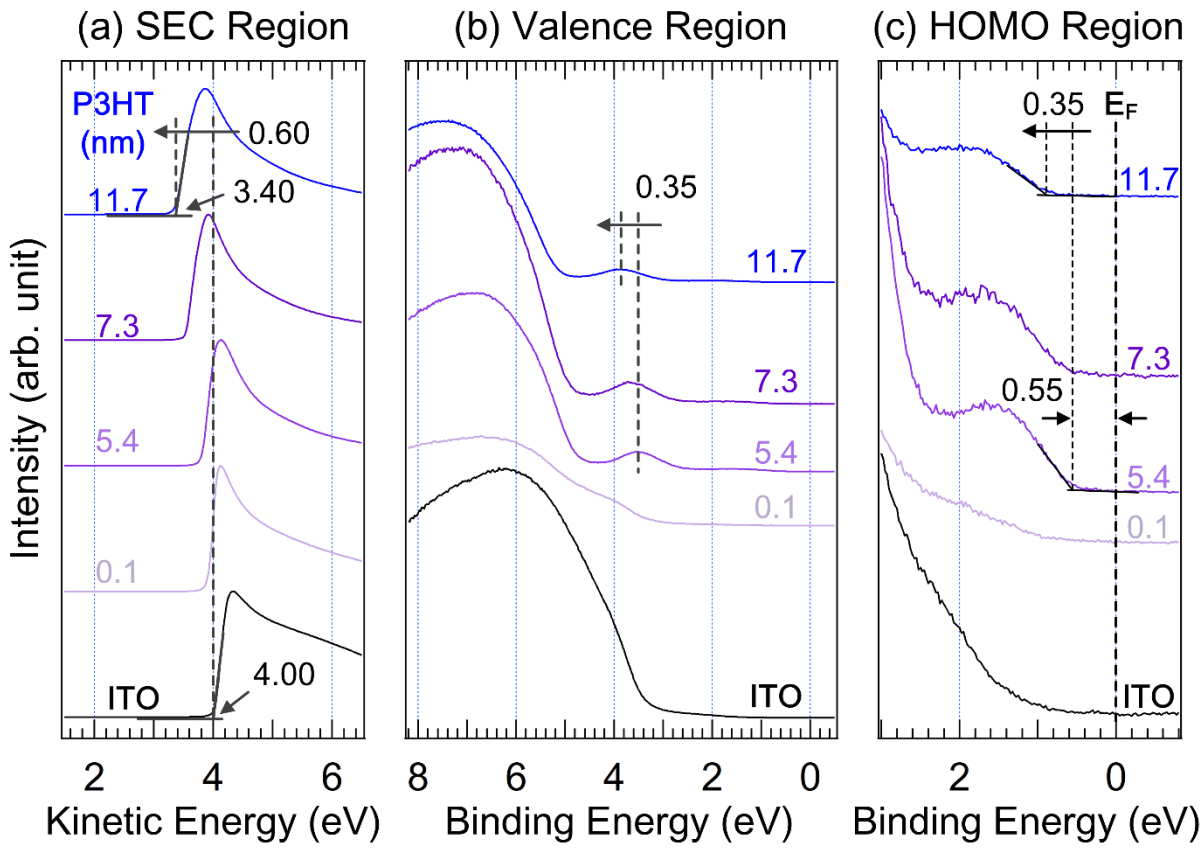

Figure S8. UPS spectra of P3HT (0.1, 5.4, 7.3, 11.7 nm) on the ITO substrate, (a) the normalized SEC region, the background and He I_β satellite-removed (b) valence region and (c) HOMO region.

7. Transport gap of CuSCN using UPS-IPES combined measurements

Figure S9 shows the UPS and IPES spectra of the CuSCN film (100 nm) on the ITO substrate. IPES measurements were carried out using a low energy electron gun with a BaO cathode and a band pass filter of 9.5 eV in the isochromat mode. The total broadening of IPES was 0.45 eV, which is calculated from the half-width of the Fermi edge of cleaned Al. The UPS and IPES spectra were plotted with respect to the E_F after proper intensity-scaling. The conduction band minimum (CBM) and valence band minimum (VBM) of CuSCN were observed at -2.90 eV and 0.75 eV, respectively. The transport gap of CuSCN was evaluated to be 3.65 eV.

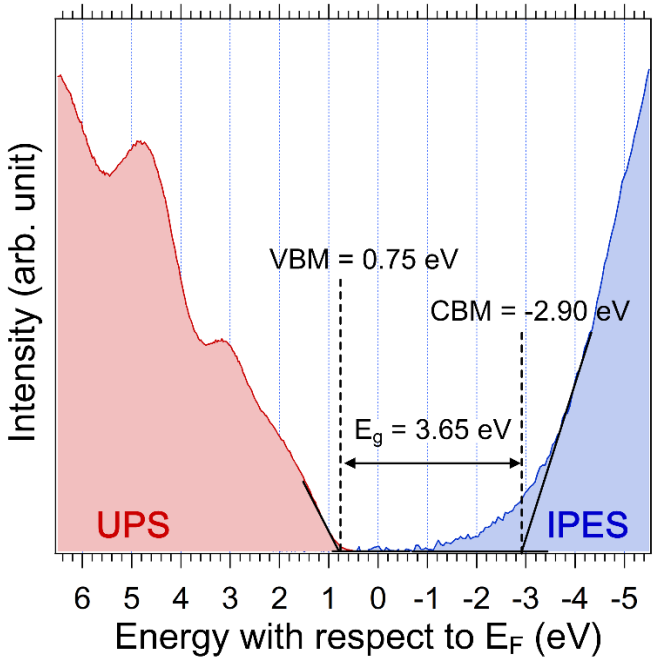

Figure S9. UPS and IPES spectra of the CuSCN film on the ITO substrate.

References

(1) Pattanasattayavong, P.; Yaacobi-Gross, N.; Zhao, K.; Ndjawa, G. O. N.; Li, J.; Yan, F.; O'Regan, B. C.; Amassian, A.; Anthopoulos, T. D. Hole-Transporting Transistors and Circuits Based on the Transparent Inorganic Semiconductor Copper(I) Thiocyanate (CuSCN) Processed from Solution at Room Temperature. *Adv. Mater.* **2013**, *25*, 1504–1509.

(2) Pattanasattayavong, P.; Ndjawa, G. O. N.; Zhao, K.; Chou, K. W.; Yaacobi-Gross, N.; O'Regan, B. C.; Amassian, A.; Anthopoulos, T. D. Electric Field-Induced Hole Transport in Copper(I) Thiocyanate (CuSCN) Thin-Films Processed from Solution at Room Temperature. *Chem. Commun.* **2013**, *49*, 4154–4156.

(3) Jaffe, J. E.; Kaspar, T. C.; Droubay, T. C.; Varga, T.; Bowden, M. E.; Exarhos, G. J. Electronic and Defect Structures of CuSCN. *J. Phys. Chem. C* **2010**, *114*, 9111–9117.

(4) Perera, V. P. S.; Senevirathna, M. K. I.; Pitigala, P. K. D. D. P.; Tennakone, K. Doping CuSCN Films for Enhancement of Conductivity: Application in Dye-Sensitized Solid-State Solar Cells. *Sol. Energy Mater. Sol. Cells* **2005**, *86*, 443–450.

(5) Smith, D.; Saunders, V. Preparation and Structure Refinement of the 2H Polytype of-Copper (I) Thiocyanate. *Acta Crystallogr. Sect. B* **1982**, *38*, 907–909.

(6) Powell, C. J.; Jablonski, A. *NIST Electron Effective-Attenuation-Length Database - Version 1.3*; National Institute of Standards and Technology: Gaithersburg, MD, 2011.